Energy & Environmental Science

COMMUNICATION

View Article Online
View Journal | View Issue

Cite this: *Energy Environ. Sci.*, 2018, **11**, 1717

Received 3rd February 2018,
Accepted 20th April 2018

DOI: 10.1039/c8ee00365c

rsc.li/ees

Thermoswitchable on-chip microsupercapacitors: one potential self-protection solution for electronic devices†

Panpan Zhang, ‡[ab] Jinhui Wang, ‡[cd] Wenbo Sheng, ‡[be] Faxing Wang, [ab] Jian Zhang, [ab] Feng Zhu, [cd] Xiaodong Zhuang,*[ab] Rainer Jordan,[be] Oliver G. Schmidt[bcd] and Xinliang Feng*[ab]

Efficient thermal protection is of great significance for electronic devices. Herein, we demonstrate a novel thermoswitchable microsupercapacitor (TS-MSC) with the self-protection function utilizing the thermodynamic behavior of a smart electrolyte, a lithium salt–dissolved polymer sol, poly(*N*-isopropylacrylamide)-*g*-methylcellulose. Benefiting from the reversibility of ionic conductivity, the TS-MSC exhibited a broad temperature window (30–80 °C) and totally switch-off behavior at 80 °C, as well as excellent cycling stability upon heating/cooling cycles. In addition, the thermal protection of on-chip integrated MSCs in series or parallel was achieved by controlling a single TS-MSC connected with a computer CPU under different working conditions. Therefore, TS-MSCs are promising components in the thermal protection of practical on-chip electronic devices.

Broader context

As a result of rapid heat generation and accumulation in a limited space, thermal runaway in integrated micro-electronic devices including microsupercapacitors possibly causes thermal damage to sensitive electronic components and brings safety hazards. In addition, running at high temperature can significantly decrease their lifespan and cause current leakage. In this respect, thermoswitchable microsupercapacitors (TS-MSCs) that feature a reversibly and sensitively temperature-dependent capacitive performance are appealing functional units for realizing thermal protection toward miniaturized electronic devices. Here this study demonstrates the rational design and a universal strategy for fabricating a TS-MSC with thermal self-protection based on temperature-dependent thermodynamic behavior of a smart electrolyte. In order to evaluate the thermal-protection function of MSC arrays for practical needs, on-chip MSCs in series or parallel are fabricated and thermal protection was realized using a single TS-MSC unit. Thus, integrating TS-MSC arrays into on-chip electronics is potentially attractive for thermal self-protection of the whole miniaturized on-chip electronic devices for practical application.

In recent years, the development of modern electronics has concentrated on some key aspects including miniaturization, lightweight, high performance, and safety issues.[1–5] However, high-performance electronics always require fast energy consumption and/or high power delivery, which will lead to spontaneous heat generation, cause thermal damage to sensitive electronic components and bring safety hazards.[6–8] In addition, running at high temperature can significantly decrease their lifespan and cause current leakage.[9–11] In general, the operating temperatures of processors and circuit boards in a mobile phone or computer should be critically controlled to be below 80 °C.[11] Previous studies on preventing thermal runaway have been focused on using thermally controlled functional modules, such as louvers, radiator fins, and cooling fans.[12–14] Nevertheless, these modules are not suitable for on-chip electronics due to the space limitation, process complexity, and cost efficiency. Thus a rational design of thermal control systems towards high performance, safe on-chip electronics is highly attractive.

In-plane microsupercapacitors (MSCs) are promising micro-sized power sources for on-chip electronics, with the advantages of ultrahigh power density, fast rate capability, and excellent cycling lifetimes.[15–28] For instance, MSCs based on alternating stacked graphene-conducting polymer compact films displayed an ultrahigh power density of 200 W cm^{-3}.[29] Silicon-wafer-supported carbide-derived carbon films delivered a high areal capacitance of 240 mF cm^{-2} in 1 M H_2SO_4.[30–32] However, high-performance MSCs are generally not responsive to physical or chemical stimuli. Inspired by smart devices with multiple

[a] *Chair for Molecular Functional Materials, Department of Chemistry and Food Chemistry, School of Science, Technische Universität Dresden, Mommsenstr. 4, 01069 Dresden, Germany. E-mail: xiaodong.zhuang@tu-dresden.de, xinliang.feng@tu-dresden.de*
[b] *Center for Advancing Electronics Dresden (cfaed), Technische Universität Dresden, 01062 Dresden, Germany*
[c] *Material Systems for Nanoelectronics, Chemnitz University of Technology, Reichenhainer Str. 70, 09107 Chemnitz, Germany*
[d] *Institute for Integrative Nanosciences, IFW Dresden, 01069 Dresden, Germany*
[e] *Chair for Macromolecular Chemistry, Department of Chemistry and Food Chemistry, School of Science, Technische Universität Dresden, Mommsenstr. 4, 01069 Dresden, Germany*

† Electronic supplementary information (ESI) available: Experimental details and supplementary figures. See DOI: 10.1039/c8ee00365c

‡ These authors contributed equally to this work.

functionalities, embedding MSCs with reversible and sensitive thermal response opens the opportunity to realize intelligent thermal protection towards miniaturized electronic devices.

In this work, we demonstrate a thermoswitchable MSC (TS-MSC) with the thermal self-protection function for on-chip electronics utilizing the thermodynamic behavior of a smart electrolyte, a lithium salt–dissolved polymer sol, poly(*N*-isopropylacrylamide)-*g*-methylcellulose. Benefiting from the reversible change in its ionic conductivity, the resultant MSC achieved 100% switch-off of the capacitance when reaching 80 °C and completely restored at room temperature upon cooling, as well as excellent reversibility upon heating–cooling cycles. Given that the critical working temperature of a computer CPU is 80 °C, the thermal protection of the CPU was revealed with on-chip TS-MSC arrays under different conditions.

The fabrication process of a TS-MSC is illustrated in Fig. 1a. First, designed patterns of Au/Cr interdigital electrodes were manufactured on clean substrates such as a Si wafer (thickness of the SiO_2 layer: 1 μm) and a flexible polyimide (PI) film, through photolithography. Then, electrochemical deposition was carried out to prepare a poly(3,4-ethylenedioxythiophene) (PEDOT) film on patterned Au-interdigital electrodes. To achieve a thermoresponsive function, a thermoresponsive graft copolymer, namely poly(*N*-isopropylacrylamide)-*g*-methylcellulose (PNIPAAm/MC), mixed with lithium chloride (LiCl, 0.1 M) was used as the electrolyte (PNIPAAm/MC/LiCl) and drop-coated on the surfaces of the interdigital electrodes to manufacture a PEDOT-based in-plane MSC (also named a TS-MSC) (Fig. S1, ESI†). For comparison, a PEDOT-based in-plane MSC with conventional polyvinyl alcohol and lithium chloride (PVA/LiCl) gel electrolyte (named a C-MSC) was also fabricated through the same procedure.

The graft copolymer PNIPAAm/MC was synthesized through free radical polymerization using NIPAAm as the monomer grafted onto MC, ammonium persulfate as an initiator, and *N*,*N*,*N*′,*N*′-tetramethylethylenediamine as an accelerator (Fig. S2, ESI†). The prepared PNIPAAm/MC solution (0.1 M) can reversibly transform between a transparent liquid state and a white hydrogel state upon heating and cooling cycles (Fig. 2a), which is further demonstrated by the decrease of transmittance using *in situ* UV-vis measurements from 25 to 85 °C during the sol–gel transition (Fig. S3, ESI†). The inflection point of the sol–gel transition is around 60 °C at 600 nm (Fig. 2b). Thus, the temperature range of the sol–gel transition fits well with the real working conditions under overheating below the boiling point of the aqueous electrolyte.

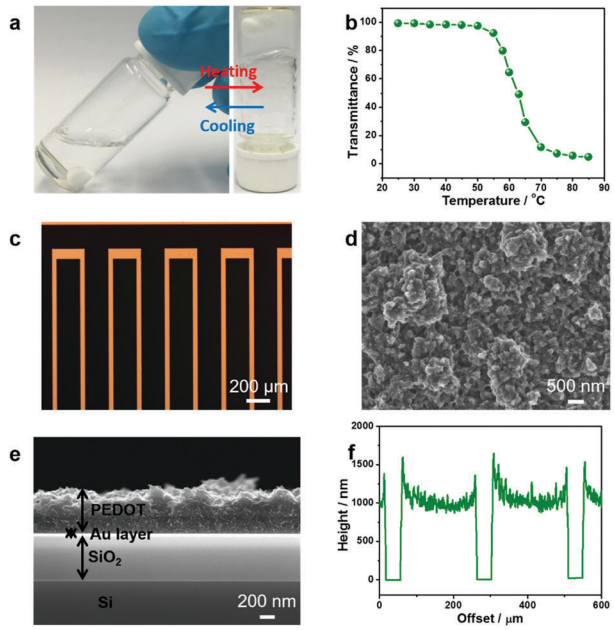

Fig. 2 Electrolyte, electrodes, and configuration of the as-fabricated TS-MSC. (a) Digital photographs of reversible sol–gel transition of PNIPAAm/MC solution by heating and cooling between 30 and 80 °C. (b) Temperature-dependent transmittance of PNIPAAm/MC solution at 600 nm. (c) An optical microscope image of a PEDOT-based MSC shows interdigital Au fingers of width 200 μm spaced 50 μm apart. The dark area corresponds to electrochemically polymerized PEDOT and the light area is the silicon wafer. Top-view (d) and profile (e) SEM images of a PEDOT film on a Si-wafer-supported Au electrode. (f) Section analysis of the PEDOT-based MSC.

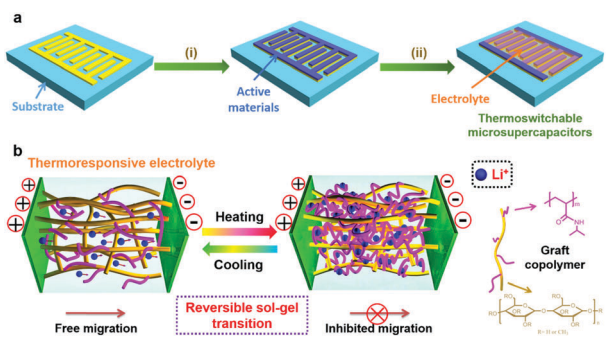

Fig. 1 Design and fabrication of a TS-MSC. (a) Schematic illustration of the fabrication of a TS-MSC on both a Si wafer and a PI film. The fabrication process includes patterning interdigital gold current collectors through photolithography, preparation of active material (PEDOT) layers through an electrodeposition method (i), and drop-casting of a LiCl-dissolved PNIPAAm/MC solution as thermoresponsive electrolyte (ii). (b) Illustration of the reversible sol–gel transition for the thermoresponsive electrolyte and ion transport between interdigital electrodes under heating and cooling.

To optimize the preparation of electrolyte, the effects of the anion type and concentration on the sol–gel transition temperature were first examined by *in situ* UV-vis spectroscopy (Fig. S4, ESI†). The inflection point of the sol–gel transition remained unchanged for the copolymer when mixed with LiCl. Furthermore, the transition temperature only shifted one degree with different LiCl concentrations (0.1, 0.5, 1 M). Interestingly, the inflection points of the sol–gel transition increased from 60 to 63 °C (0.1 M), 66 °C (0.5 M), and 70 °C (1 M) for the copolymer mixed with lithium acetate (CH_3COOLi), but greatly from 60 to 75 °C (0.1 M), 79 °C (0.5 M), and 82 °C (1 M) for the copolymer with lithium perchlorate ($LiClO_4$). Unlike chloride ions, acetate and perchlorate ions inhibited the formation of hydrogels. Thus the subsequent concentration (0.1 M) of LiCl was chosen for the electrolyte, unless specified otherwise. The thermoresponsive mechanism of PNIPAAm/MC/LiCl based on reversible sol–gel transition at different temperatures (heating/cooling) is illustrated in Fig. 1b. During the heating treatment,

side-chain PNIPAAm collapses and forms hydrogels through hydrophobic association (Fig. 2a), which can thus inhibit the migration of Li^+ ions between the electrodes. When turning to the cooling process, such a copolymer can easily stretch back into a relaxed state because of the formation of hydrogen bonds between *N*-isopropyl groups and water.[33]

Because of the high molar mass of the monomer and low doping level, PEDOT exhibits low specific capacitance relative to other conducting polymers (*e.g.*, polyaniline and polypyrrole).[34] However, PEDOT shows electrochemical activity in a wide potential window in different electrolytes (aqueous, organic, and ionic liquids).[35] The morphology of the fabricated PEDOT-based MSC was inspected through scanning electron microscopy (SEM) and high-resolution transmission electron microscopy (HRTEM). Patterned gold interdigital current collectors on a Si wafer and a PI film are presented in Fig. S5 (ESI†). In addition, the magnified SEM image shows the porous morphology of PEDOT (Fig. 2d) generated during the electrochemical deposition, which was also confirmed through HRTEM investigations (Fig. S6, ESI†). The side-view SEM image of the PEDOT film on the Si wafer reveals that the thickness of the PEDOT layer is 1 ± 0.2 μm (Fig. 2e and f). Therefore, the PEDOT layer over the gold interdigital electrodes has uniform electrochemical deposition without obvious cracking or delamination (Fig. 2c). Furthermore, energy-dispersive spectroscopy (EDS) elemental mapping analysis of top-view and side-view SEM images manifests the well-patterned electrodes, well-grown PEDOT, and distinct element distribution (Fig. S7 and S8, ESI†). The width and gap of the interdigital Au fingers are 200 and 50 μm, respectively. A wafer-scale MSC array with a PEDOT layer (10×10) was successfully fabricated by facile, low-cost photolithography and electrodeposition (Fig. S9, ESI†), which offers promising prospects for up-scalable production of on-chip functional power sources.

Cyclic voltammetry (CV) measurements were first performed to evaluate the electrochemical performance of the as-fabricated TS-MSC at room temperature. Before assembling the TS-MSC, the active material of PEDOT was examined in a standard three-electrode cell (Fig. S11, ESI†). The CV curves of the TS-MSC at different scan rates (Fig. S12a, ESI†) displayed an ideal rectangular shape, ascribed to the formation of electrochemical double layers and also fast redox reactions such as doping/dedoping processes at the surfaces of the electrodes. The capacitive behavior of the TS-MSC was further studied through galvanostatic charge–discharge (GCD) measurements at current densities from 0.02 to 1 mA cm^{-2} (Fig. S12b and c, ESI†). According to the GCD curves, the areal and volumetric capacitances (C_A and C_V) were calculated (Fig. S12d, ESI†) to be 2.4 mF cm^{-2} and 25 ± 5 F cm^{-3}, respectively, at a current density of 20 μA cm^{-2}. Moreover, the TS-MSC exhibited long-term stability with 88% capacitance retention up to 5000 charge–discharge cycles at 0.1 mA cm^{-2}, confirmed by the unchanged electrochemical impedance spectra (EIS) before and after the cycling measurement (Fig. S12e and f, ESI†). The effect of bending on the performance of a PI-supported TS-MSC was examined using CV curves under different bending states (Fig. S13, ESI†) and no obvious changes were observed, highlighting the good flexibility and electrochemical stability of the PI-supported MSC for flexible microdevices.

To determine the thermoresponsive behavior of the TS-MSC, its temperature-dependent electrochemical performance was studied. For comparison, conventional MSCs using PVA/LiCl (C-MSC) electrolytes were also fabricated and investigated under the same conditions. Clearly, the areas of the CV curves of the TS-MSC decreased (approximately 20% at 40 °C, 30% at 50 °C, 40% at 60 °C, 90% at 70 °C, and 100% at 80 °C) upon increasing the temperature from 30 to 80 °C at the same scan rate of 200 mV s^{-1}. This is because the sol–gel transition of the electrolyte restrains the migration of Li^+ ions (Fig. 3a, Fig. S14 and S15, ESI†). Notably, charging and discharging could not be realized at all when reaching 80 °C, suggesting a complete switch-off behavior of the thermal protection. In contrast, upon increasing the temperature from 30 to 80 °C, the areas of the CV curves of the C-MSC increased, which could be attributed to the increase in the diffusion velocity of Li^+ ions in the electrolyte (Fig. S16 and S17, ESI†). In addition, the GCD curves of the TS-MSC from 30 to 70 °C exhibited a dramatic decrease in the charge–discharge time (Fig. 3b and Fig. S18–S21, ESI†), which is associated with the temperature-controlled electrochemical behavior.

To identify the reason for the temperature-dependent performance drop, the ionic conductivity of the thermoresponsive electrolyte (PNIPAAm/MC/LiCl, Fig. 3c and Fig. S22, ESI†) was measured. It showed a three order of magnitude decrease from the sol (10 mS cm^{-1}) to gel (3.4×10^{-2} mS cm^{-1}) state, confirming the restriction of ion transport in the gel matrix at a temperature above 80 °C. The Li^+ ions and solvent can be easily encapsulated within the local polymer matrix without long-range migration. Moreover, the EIS for the TS-MSC and C-MSC were analyzed (Fig. 3d–f). At low frequency, the curves for the TS-MSC presented much lower slopes than those in the higher temperature range, again proving that the electrode had a much higher ion diffusion resistance upon heating. In contrast, the C-MSC exhibited a slightly increased slope upon

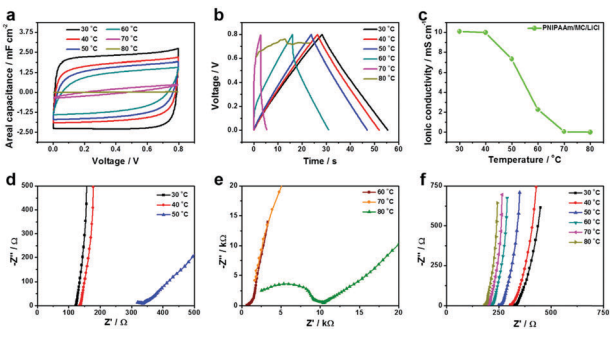

Fig. 3 Comparison of the electrochemical performances of the TS-MSC and C-MSC. (a) CV curves and (b) GCD curves of the TS-MSC in the 30–80 °C temperature range. (c) Ionic conductivities of the thermoresponsive PNIPAAm/MC/LiCl electrolyte upon increasing the temperature from 30 to 80 °C. Nyquist plots of the (d and e) TS-MSC and (f) C-MSC upon increasing the temperature from 30 to 80 °C.

increasing the temperature from 30 to 80 °C. At high frequency, large radius semicircles were observed with increase in temperature of the TS-MSC, suggesting an increase in the impendence controlled by charge transfer on the electrode surface.[36] In addition, new MSCs based on electrodeposited polypyrrole were constructed and efficient thermoresponsive behavior was achieved using the same thermoresponsive electrolyte, confirming the universal strategy for TS-MSCs (Fig. S27, ESI†).

We then studied the *in situ* thermal response of the TS-MSC with GCD measurements (Fig. 4a). To demonstrate the effect of sol–gel transition on the capacitive performance of the TS-MSC, the areal capacitance at a variety of temperatures was calculated from the GCD curves, as shown in Fig. 4b. It decreased gradually from 1.83 mF cm^{-2} at 30 °C to 1.78 mF cm^{-2} at 40 °C, and 1.60 mF cm^{-2} at 50 °C. A sharp decrease from 1.43 mF cm^{-2} at 60 °C to 0.66 mF cm^{-2} at 70 °C, and 0 mF cm^{-2} at 80 °C was observed. This result is consistent with the changes in the UV-vis transmittance (600 nm) of 98% at 40 °C, 97% at 50 °C, 65% at 60 °C, 11% at 70 °C, and 0% at 80 °C of sol–gel phase transition (Fig. 2b and Fig. S3, ESI†). It should be noted that either narrow temperature ranges or low fading percentages of specific areal capacitance have been reported thus far for thermoresponsive energy storage devices (Table 1),[7,36–39] which mainly suffered from the irreversible aggregation or macrogel formation of block copolymers with respect to the temperature changes.

The dependence of phase angles on the frequencies reflects the response time of the TS-MSC (Fig. 4c). The characteristic frequency f_0 at a phase angle of −45° for the TS-MSC at 30 °C was 8.4 Hz, which is much higher than the values for devices operated at higher temperatures. Thus the corresponding time constant τ_0 ($\tau_0 = 1/f_0$), which refers to the minimum time required to discharge all the energy from the device with an efficiency of more than 45%, was calculated to be 0.12 s for the TS-MSC at 30 °C compared with 0.15 s at 40 °C, 0.34 s at 50 °C, and 0.69 s at 60 °C. To demonstrate the reversibility of the TS-MSC, GCD experiments were performed at varied temperatures by heating the electrolyte from 30 to 80 °C, and cooling down. The specific capacitance did not fade over repeated heating and cooling for 50 cycles (Fig. 4d). These results supported that the thermoswitchable TS-MSC had excellent reversibility by temperature variation.

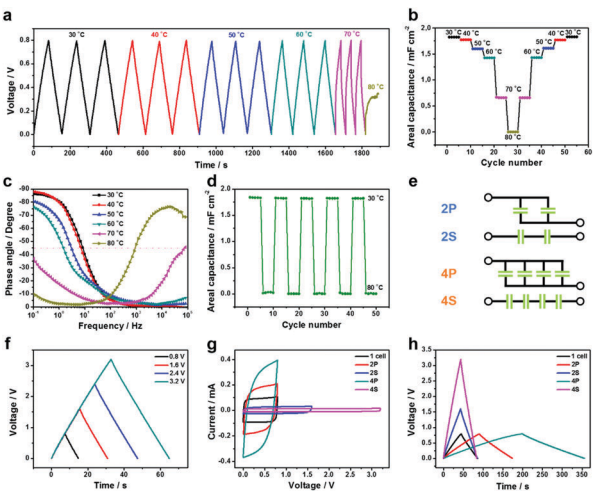

Fig. 4 Thermoresponsive behavior of TS-MSCs. (a) GCD curves at different temperatures from 30 to 80 °C. (b) Areal capacitance as a function of temperature from 30 to 80 °C at a current density of 20 μA cm^{-2}. (c) Impedance phase angle as a function of frequency for TS-MSCs in the 30–80 °C temperature range. (d) Reversible areal capacitance behavior of TS-MSCs with sol–gel transition for 50 heating–cooling cycles. (e) Circuit diagrams of two and four TS-MSCs connected in series and parallel. (f) GCD curves of TS-MSCs with four units connected in series at a current density of 60 μA cm^{-2}. (g) CV curves at a scan rate of 200 mV s^{-1} and (h) GCD curves at a current density of 40 μA cm^{-2} for TS-MSCs with two and four units connected in series and parallel at room temperature.

Because of the microscale size, a single device can only provide a limited power, which cannot meet the demand for most practical applications. It is a commonly used approach to connect individual units in series and parallel to achieve the required specific voltage and capacitance. The circuit diagrams of two and four TS-MSCs connected in parallel and series are presented in Fig. 4e. For example, the TS-MSC array with four units connected in series reaches a high operational voltage of 3.2 V (Fig. 4f, Fig. S28 and S29, ESI†). The TS-MSC array in a parallel configuration exhibits an enhanced capacitance for two and four units compared with that of a single unit (Fig. 4g). Furthermore, the two and four units connected in series result in an extended potential window of up to 1.6 and 3.2 V, respectively. Similarly, the charge–discharge curves were also recorded for the two and four units connected in series and parallel compared with that for a single unit (Fig. 4h).

As an important component for on-chip electronics, the CPU panel faces considerable heat generation/accumulation under heavy running load, which ultimately leads to the fading of their performance and lifetime. Therefore, it is of great concern to protect the electronics against the high temperature. Thus here we studied the real-time temperature change of a computer CPU operating under standby, working, and overloaded conditions using a non-contact infrared thermometer (Fig. S30, ESI†). As shown in Fig. 5a and d, the working temperatures of the CPU panel are in the 30–80 °C range, matching well with that of a single TS-MSC. Therefore, we analyzed the thermoresponsive performance of TS-MSC arrays in series and in parallel connected with a computer CPU under different working conditions.

For the TS-MSC array in series on the CPU panel, the areas of the CV curves decreased when the temperature was increased from 30 to 80 °C (Fig. 5b, Fig. S31 and S32, ESI†). At 60 °C, only approximately 50% of the initial areal capacitance was retained. No charge–discharge current was observed at 80 °C, suggesting the efficient protection of the entire MSC array in series. In addition, the GCD curves of MSCs further confirmed the decrease of the charge–discharge time when increasing the CPU temperature from 30 to 80 °C (Fig. 5c, Fig. S33 and S34, ESI†). This demonstrated the excellent switch on/off behavior of the entire array in series through a single unit. To further verify the control of the MSC array in parallel with thermal self-protection, CV testing and GCD measurements were performed (Fig. 5e and f, Fig. S35–S38, ESI†). A gradual decrease was

Table 1 Thermoresponsive performance of supercapacitors

Type of supercapacitor	Active material	Thermoresponsive polymer	Switch-off temperature	Fading percentage	Cycling stability	Ref.
Three-electrode	Polyaniline	Poly(*N*-isopropylacrylamide-*co*-acrylic acid) (pNcA)	50	85%	—	38
Three-electrode	NiAl-layered double hydroxide	Poly(*N*-isopropylacrylamide-*co*-2-acrylamido-2-methyl propane sulfonic acid) (P(NIPAM-*co*-SPMA))	40	93%	—	7
Coin-type cell	Carbon nanotubes	Poly(*N*-isopropylacrylamide-*co*-acrylamide) (PNIPAM/AM)	70	65%	—	36
Coin-type cell	Polypyrrole or activated carbon	Poly(ethylene oxide)-*block*-poly(propylene oxide)-*block*-poly(ethylene oxide) (PEO–PPO–PEO)	60	Nearly 100%	—	39
Microsupercapacitor	Poly(3,4-ethylenedioxy thiophene) or polypyrrole	Poly(*N*-isopropylacrylamide)-*g*-methylcellulose (PNIPAAm/MC)	80	100%	50	This work

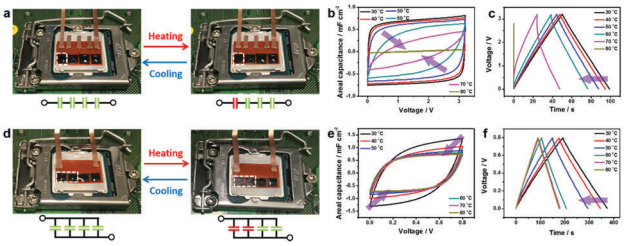

Fig. 5 Thermoresponsive behavior of TS-MSC arrays physically connected on a computer CPU panel under different working conditions. Digital photographs and circuit diagrams of four TS-MSCs connected (a) in series and (d) in parallel. The white-dotted box represents the TS-MSC unit and the other units in the MSC array are the C-MSCs. The red and green symbolic capacitors represent the capacitors with switch-on and switch-off states, respectively. Comparison of (b) CV curves at a scan rate of 500 mV s^{-1} and (c) GCD curves at a current density of 40 μA cm^{-2} for four TS-MSCs connected in series in the 30–80 °C temperature range. Comparison of (e) CV curves at a scan rate of 500 mV s^{-1} and (f) GCD curves at a current density of 40 μA cm^{-2} for four TS-MSCs connected in parallel in the 30–80 °C temperature range.

observed from 30 to 60 °C. Starting from 60 °C, the anodic and cathodic currents remained stable in the CV curves. The area of the CV curve at 80 °C decreased by almost half of that at 30 °C. Moreover, the device array exhibited a constant decrease in the charge–discharge time, retaining the areal capacitance of two units. It means that the heated TS-MSC unit can switch on/off itself and achieve efficient thermal control over the TS-MSC array in parallel.

Conclusions

In summary, we have demonstrated a photolithographically fabricated MSC with a reversible thermoresponsive self-protection function based on a sol–gel transition of the electrolyte. The heating-induced gelation of the graft copolymer-based electrolyte inhibits the migration of Li^+ ions while the solubilization in the cooling state recovers the free migration of Li^+ ions. Benefiting from the reversible changes in ionic conductivity, the TS-MSC exhibited a broad temperature window (30–80 °C) and totally switch-off behavior at 80 °C, as well as excellent cycling stability upon heating/cooling cycles. The efficient switch on/off capability demonstrates its great potential in realizing real-time self-protection for temperature-sensitive components through integration with TS-MSC arrays. In addition, the thermal protection of on-chip integrated MSCs in series or parallel can be achieved by controlling a single TS-MSC connected with a computer CPU under different working conditions. This work offers an effective way in the design of thermoresponsive micropower devices, *e.g.* microbatteries, microfuel cells, and other energy microsystems. Furthermore, such functional MSCs provide an attractive solution to address the safety concerns of the nowadays portable on-chip electronic devices for potential applications such as smart electronics, biomimetics, and healthcare devices.

Conflicts of interest

There are no conflicts to declare.

Acknowledgements

This work was supported by the German Research Foundation (DFG) within the Cluster of Excellence 'Center for Advancing Electronics Dresden' (cfaed) and financed by the Initiative and Networking Fund of the German Helmholtz Association, the International Helmholtz Research School for Nanoelectronic Networks NanoNet (VH-KO-606), an ERC Grant on 2DMATER and the EU Graphene Flagship. The authors thank Dr Gang Wang and Dr Sheng Yang for helpful discussions. We also acknowledge the use of the facilities in the Dresden Center for Nanoanalysis (DCN) of Technische Universität Dresden.

Notes and references

1 H. Sun, Y. Zhang, J. Zhang, X. Sun and H. Peng, *Nat. Rev. Mater.*, 2017, **2**, 17023.
2 M. R. Lukatskaya, B. Dunn and Y. Gogotsi, *Nat. Commun.*, 2016, **7**, 12647.
3 X. Wang, Y. Chen, O. G. Schmidt and C. Yan, *Chem. Soc. Rev.*, 2016, **45**, 1308.
4 Y. Zheng, Y. Yang, S. Chen and Q. Yuan, *CrystEngComm*, 2016, **18**, 4218.
5 Z. Lou, L. Li, L. Wang and G. Shen, *Small*, 2017, **13**, 1701791.
6 Y. Huang, M. Zhu, Y. Huang, Z. Pei, H. Li, Z. Wang, Q. Xue and C. Zhi, *Adv. Mater.*, 2016, **28**, 8344.
7 Y. Dou, T. Pan, A. Zhou, S. Xu, X. Liu, J. Han, M. Wei, D. G. Evans and X. Duan, *Chem. Commun.*, 2013, **49**, 8462.

8 Y. Yang, D. Yu, H. Wang and L. Guo, *Adv. Mater.*, 2017, **29**, 1703040.
9 G. Xiong, A. Kundu and T. S. Timothy, *Thermal Effects in Supercapacitors*, Springer International Publishing, Germany, 2015.
10 R. Kötz, M. Hahn and R. Gallay, *J. Power Sources*, 2006, **154**, 550.
11 N. Vichare, P. Rodgers, V. Eveloy and M. G. Pecht, *IEEE Trans. Device Mater. Reliab.*, 2004, **4**, 658.
12 R. Mongia, A. Bhattacharya and H. Pokharna, *Microelectron. J.*, 2008, **39**, 992.
13 M. Jaworski, *Appl. Therm. Eng.*, 2012, **35**, 212.
14 E. Walsh, R. Grimes and P. Walsh, *Appl. Therm. Eng.*, 2010, **30**, 2363.
15 D. Yu, K. Goh, H. Wang, L. Wei, W. Jiang, Q. Zhang, L. Dai and Y. Chen, *Nat. Nanotechnol.*, 2014, **9**, 555.
16 M. F. El-Kady and R. B. Kaner, *Nat. Commun.*, 2013, **4**, 1475.
17 Z. S. Wu, K. Parvez, X. Feng and K. Müllen, *Nat. Commun.*, 2013, **4**, 2487.
18 J. Lin, Z. Peng, Y. Liu, F. Ruiz-Zepeda, R. Ye, E. L. Samuel, M. J. Yacaman, B. I. Yakobson and J. M. Tour, *Nat. Commun.*, 2014, **5**, 5714.
19 M. F. El-Kady, M. Ihns, M. Li, J. Y. Hwang, M. F. Mousavi, L. Chaney, A. T. Lech and R. B. Kaner, *Proc. Natl. Acad. Sci. U. S. A.*, 2015, **112**, 4233.
20 N. A. Kyeremateng, T. Brousse and D. Pech, *Nat. Nanotechnol.*, 2017, **12**, 7.
21 M. Beidaghi and Y. Gogotsi, *Energy Environ. Sci.*, 2014, **7**, 867.
22 D. Qi, Y. Liu, Z. Liu, L. Zhang and X. Chen, *Adv. Mater.*, 2017, **29**, 1602802.
23 A. Tyagi, K. M. Tripathi and R. K. Gupta, *J. Mater. Chem. A*, 2015, **3**, 22507.
24 L. Liu, Z. Niu and J. Chen, *Nano Res.*, 2017, **10**, 1524.
25 G. Xiong, C. Meng, R. G. Reifenberger, P. P. Irazoqui and T. S. Fisher, *Electroanalysis*, 2014, **26**, 30.
26 Z.-S. Wu, X. Feng and H.-M. Cheng, *Natl. Sci. Rev.*, 2014, **1**, 277.
27 P. Zhang, F. Zhu, F. Wang, J. Wang, R. Dong, X. Zhuang, O. G. Schmidt and X. Feng, *Adv. Mater.*, 2016, **29**, 1604491.
28 H. Wang, B. Zhu, W. Jiang, Y. Yang, W. R. Leow, H. Wang and X. Chen, *Adv. Mater.*, 2014, **26**, 3638.
29 Z. S. Wu, K. Parvez, S. Li, S. Yang, Z. Liu, S. Liu, X. Feng and K. Müllen, *Adv. Mater.*, 2015, **27**, 4054.
30 P. Huang, C. Lethien, S. Pinaud, K. Brousse, R. Laloo, V. Turq, M. Respaud, A. Demortière, B. Daffos, P. L. Taberna, B. Chaudret, Y. Gogotsi and P. Simon, *Science*, 2016, **351**, 691.
31 X. Zhuang and X. Feng, *Angew. Chem., Int. Ed.*, 2016, **55**, 6136.
32 B. Anasori, M. R. Lukatskaya and Y. Gogotsi, *Nat. Rev. Mater.*, 2017, **2**, 16098.
33 C. d. l. H. Alarcón, S. Pennadam and C. Alexander, *Chem. Soc. Rev.*, 2005, **34**, 276.
34 G. A. Snook and G. Z. Chen, *J. Electroanal. Chem.*, 2008, **612**, 140.
35 N. Kurra, M. K. Hota and H. N. Alshareef, *Nano Energy*, 2015, **13**, 500.
36 H. Yang, Z. Liu, B. K. Chandran, J. Deng, J. Yu, D. Qi, W. Li, Y. Tang, C. Zhang and X. Chen, *Adv. Mater.*, 2015, **27**, 5593.
37 J. C. Kelly, N. L. Degrood and M. E. Roberts, *Chem. Commun.*, 2015, **51**, 5448.
38 J. C. Kelly, M. Pepin, D. L. Huber, B. C. Bunker and M. E. Roberts, *Adv. Mater.*, 2012, **24**, 886.
39 Y. Shi, H. Ha, A. Al-Sudani, C. J. Ellison and G. Yu, *Adv. Mater.*, 2016, **28**, 7921.

